

Acknowledgments

During my days as a graduate student in the Institute of Nanotechnology, National Chiao Tung University, many peoples have contributed their wisdom and advice to me. I thank them all for helping me to produce this Thesis.

I am particularly grateful to my advisors, Dr. Fu-Hsiang Ko, who have always patiently guided and encouraged me. I have benefited a lot from their vision and advice, not only with respect to my studies but also with life's experiences. My appreciation is also extended to the members of my oral defense committee for all of their valuable suggestions.

The help I have received from, and the discussions I have had with, my colleagues are too numerous to list in detail. I am grateful to my classmates in the Institute of Nanotechnology, including Kun-Lin Li, Chi-Wei Chiu, Chien-Wen Huang and I-Chieh Hsu. I cherish the time that we shared together. I also thank the members of National Nano Device Laboratories, including Hsin-Yen Huang, Chun-Chi Chen, Chi-Chang Wu and Shu-Chun Cheng for their support with the instrumentation facilities and experimental procedures.

Finally, to my family, my most devoted supporters: Thanks for your patience and understanding.

陽極氧化鋁模板自組裝金屬氧化物奈米點陣列


研究生:吳佳典

指導教授:柯富祥 博士

國立交通大學奈米科技研究所 碩士班

摘要

近年來，研究零維奈米結構陣列的吸引與日俱增，因為他們獨特的物理和化學特性應用在例如光電、資訊儲存、量子元件和感測上面。許多不同製造奈米點的方法已經被開發，但是常常受限於材料或是製造成本上的困難。



因此，我們發展出一套新穎的方法透過陽極氧化鋁模板來自主裝產生金屬氧化物的規則奈米點陣列。以電化學的方式在陽極產生氧化鋁孔洞的同時，底層的金屬同時被氧化而在孔洞底端成長出奈米點。以草酸、硫酸和磷酸不同的電解液和不同施加電壓下觀察奈米點的陣列。製造出來的奈米點直徑可由10nm~200nm相對應密度 $10^{11}/\text{cm}^2 \sim 10^9/\text{cm}^2$ 。奈米點的大小和密度都可以透過控制施加電壓的改變來獲得控制。以掃描式電子顯微鏡、穿透式電子顯微鏡和電子能譜儀來觀察、分析，進而推測其成長的機制。利用本篇論文的製造方法可以快速的以簡單而廉價的方式製造出高密度的奈米點陣列。

Self-Organized Metal Oxide Nanodot Arrays through Anodic Alumina Template

Student : Chia-Tien Wu

Advisor : Dr. Fu-Hsiang Ko

Institute of Nanotechnology
National Chiao Tung University

Abstract

Recently, 0-D nanostructure arrays have attracted growing interest due to unique chemical and physical properties in the field of optoelectronics, information storage, quantum device and sensing. Variety of alternative methods has been proposed for the formation of nanodot arrays but most of these works can be applied to only limit material systems. A novel strategy for fabricating the ordered nanodot arrays of metal oxide with anodic alumina film to serve the template. Anodising reaction proceeds in the sequence of growth of porous anodic alumina when the aluminum layer is consumed up to the underlying metal, and the growth of metal oxide under the bottoms of the alumina pores occurred simultaneously. The nanodot diameter demonstrated here ranges between 10nm ~ 200nm and density ranges between $10^{11}/\text{cm}^2 \sim 10^9/\text{cm}^2$. Size and density of nanodot arrays can be controlled by various anodic conditions. Nanodot arrays have been investigated by scanning electron microscopy, transmission electron microscopy and X-ray photoelectron spectroscopy depth profiling hence infer the growth mechanism. High density nanodot arrays can be easily and inexpensively fabricated by the method in this thesis.

Contents

Acknowledgment-----	I
Chinese Abstract-----	II
Abstract-----	III
Contents-----	IV
List of Tables-----	VII
List of Figures-----	VIII

Chapter 1: Introduction.....	1
1.1 General Introduction.....	1
1.2 Zero-Dimensional Nanostructure.....	2
1.3 Top-Down Nanotechnology.....	3
1.4 Bottom-Up Nanotechnology.....	6
1.5 Motivation.....	9

Chapter 2: Literature Review.....	11
2.1 Anodic Aluminum Oxidation (AAO).....	11
2.2 Fabrication Technologies of Nanodot Arrays.....	17
2.2.1 Self-Assembly Copolymer / Copolymer Template.....	17
2.2.2 Stranski-Krastanow Growth.....	19
2.2.3 Chemical Colloidal Self-Assembly.....	21
2.2.4 SPM-induced Growth.....	23
2.3 Nanodot Arrays Fabricated by AAO.....	25

Chapter 3: Experimental Methods.....	28
3.1 Films Deposition.....	28
3.2 Electrochemical Process.....	30
3.3 Specimen Analysis.....	32
Chapter 4: Self-Organized TaO_x Nanodot Arrays.....	35
4.1 General Introduction.....	35
4.2 Oxalic and Sulfuric Specimen.....	37
4.2.1 Morphology of Nanodot Arrays.....	37
4.2.2 Mechanism of Growth of Nanodot Arrays.....	45
4.2.3 Composition Analysis.....	47
4.3 Phosphoric Specimen.....	51
4.3.1 Observations of Nanodot Arrays.....	51
4.3.2 Analysis of Nanodots.....	54
Chapter 5: Self-Organized ZnO Nanodot Arrays.....	57
5.1 General of Nano-Dimensional ZnO Nanostructure.....	57
5.2 Structure and Morphology of ZnO Nanodot Arrays.....	60
Chapter 6: Conclusions.....	66
Chapter 7: Future Work.....	67

References..... 68



List of Tables

Table 3-1..... 32
Anodization conditions for the preparation of metal oxide nanodot arrays.



List of Figures

Figure 1.1	3
The semiconductor industry roadmap of memory technologies and the associated lithographic technologies used to manufacture each generation of devices.	
Figure 1.2	5
The nanoimprinting process.	
Figure 1.3	6
Two basic approaches toward the fabrication of nanomaterials: top-down (from left to right) and bottom-up (from right to left).	
Figure 2-1	12
(a) Schematic drawing of the idealized structure of anodic porous alumina. (b) SEM micrographs of the bottom view of anodic alumina layers. Anodization was conducted in 0.3 M oxalic acid at 1 °C at 40 V.	
Figure 2-2	13
Expansion of aluminum during anodic oxidation. On the left the level of the unoxidized metal surface is depicted.	
Figure 2-3	14
(a) Cross-sectional SEM image of 2-mm-thick porous alumina mask anodized at 60 V for 5 min followed by a 1 h pore widening etch. The white bar is 1 mm long. (b) SEM image of barrier layer features were observed on Si. The white bar is 200 nm long.	
Figure 2-4	16
(a) Process for the fabrication of ideally ordered nanochannel array. SiC mold with hexagonally ordered array of convexes, indentation of Al with SiC mold, and anodic porous alumina. (b) SEM micrograph of surface view of ideally ordered anodic	

porous alumina and un-patterning anodic alumina.

Figure 2-5..... 18

(a) AFM image of a CdS/LSEO thin film supported on a carbon-coated silicon wafer.

(b) TEM image of a CdS/LSEO thin film after removal from carbon-coated silicon wafer with 1% HF solution.

Figure 2-6..... 19

Tapping mode AFM images of (a) Block copolymer template etched by UV exposure.

(b) Au/Cr dot arrays after eliminating PS matrix by the irradiation of UV.

Figure 2-7..... 20

(a) AFM image of an array of Ge islands on prepatterned Si (001) surfaces. (b)

Cross-sectional measurement of a typical Ge island. (c) Normal view of a histogram of the statistics of the island surface normal vectors that are measured vertically.

Figure 2-8..... 21

(a) STM image of the ordered dislocation network formed by the second Ag monolayer on Pt (111) and subsequent annealing to 800 K. The inset shows a model of this triangular strain relief pattern. (b) A superlattice of islands is formed on Ag deposition onto this network at 110 K. Inset, the Fourier transform of the STM image shows the high degree of order and the hexagonal symmetry of the nanostructure array.

Figure 2-9..... 22

(a) schematic side-view of Au nanoparticles attached to a SAM by molecular wires. (b)

TEM micrographs of monolayer films of 3.7 nm Au cluster supported on thin flake of MoS₂.

Figure 2-10 23

(a) Schematic representation of the layer construction of nanomaterials from Q-CdS particles and a dithiol. (b) TEM micrograph of AOT-capped CdS nanoparticle array.

Inset clearly shows two representative nanoparticles capped by AOT surfactant layer, with thickness of single layer ca. 14 Å.

Figure 2-11..... 24

(a) STM image of germanium islands on the silicon (111) substrate covered with 2.9 bilayer of Ge at 450°C. (b) AFM image of field-induced formation silicon oxide nanodot arrays. The dots are 40 nm apart and with an average width of 10 nm. The same tip was used to grow the dots and to image them afterwards.

Figure 2-12..... 25

(a) Schematic process used to fabricate nanodots arrays on surface using alumina template. (b) Ni nanodot arrays on Si wafer.

Figure 2-13..... 27

(a) Schematic process used to fabricate nanodots arrays on surface using alumina template. (b) Au nanodot arrays on Si wafer. (c) Au nanorod arrays produced by electrodeposition into an alumina template on a Au/Ti/Si substrate.

Figure 3-1..... 28

Experimental flowchart for the fabrications and analyses of metal oxide nanodot arrays.

Figure 3-2..... 29

Schematic diagram of fabrication of the tantalum oxide nanodot arrays: (A) prestructured sample, (B) first anodic oxidation step, (C) second anodic oxidation step and metal oxide nanodot arrays formation, and (D) metal oxide nanodot arrays after removing alumina film.

Figure 3-2..... 31

The schematic diagram of experimental setup for the aluminum electropolishing and anodization.

Figure 4-1..... 35

Top-view SEM image of the porous anodic alumina film anodizing after pore widening in 5-wt. % H_3PO_4 .

Figure 4-2..... 36

Current versus time plots produced during the anodization of aluminum films of sample J.

Figure 4-3..... 40

SEM images of tantalum oxide nanodot arrays in 1.8M sulfuric acid at (A) 5V (B) 10V (C) 15V (D) 20V (E) 25V (F)30V . The scale bar is 100 nm.

Figure 4-4..... 41

SEM images of tantalum oxide nanodot arrays in 1.8M sulfuric acid at (G) 10V (H)20V (I) 30V The scale bar is 100 nm. (J) 40V (K) 505V (L) 60V. The scale bar is 300 nm.

Figure 4-5..... 42

Slide-view SEM image of tantalum oxide nanodots arrays on the surface of sample J.

Figure 4-6..... 42

(A) cross-section SEM image of the nanodots with overlying porous alumina film, (B) after removing alumina film.

Figure 4-7..... 43

The effect of applied voltage on average diameter and density of tantalum oxide nanodots. (A) H_2SO_4 specimen. (B) $H_2C_2O_4$ specimen.

Figure 4-8..... 43

The effect of applied voltage on average distance between nanodots' center and average gap width between nanodots' bases of tantalum oxide nanodots. (A) H_2SO_4 specimen. (B) $H_2C_2O_4$ specimen.

Figure 4-9..... 46

Schematic diagrams showing the principal steps of modification of the underlying

metal / alumina interface.

Figure 4-10..... 49

XPS Ta 4f spectrum of sample J (oxalic acid in 40 V). “t” means sputtering time.

Figure 4-11..... 50

XPS Ta 4f spectrum of different sample which sputtered for 3 min.

Figure 4-12..... 52

Top-view SEM image of tantalum oxide nanodot arrays in 5wt-% phosphoric acid at 100V.

Figure 4-13..... 52

Slide-view SEM image of tantalum oxide nanodot arrays in 5wt-% phosphoric acid at 100V.

Figure 4-14..... 53

Slide-view SEM image of tantalum oxide nanodot arrays with unanodized aluminum.

Figure 4-15..... 53

Cross-section SEM image of tantalum oxide nanodot arrays with overlying porous alumina film.

Figure 4-16..... 54

TEM image of tantalum oxide nanodot array under the porous alumina film; the inset is the SAED (selected area electron diffraction) image.

Figure 4-17..... 56

Schematic diagrams showing the principal steps of modification of the underlying metal / alumina interface in phosphoric acid specimen.

Figure 5-1..... 58

(a) Wurtzite structure. (b) ~ 30nm ZnO nanodot arrays show an exciton PL line at 375 nm with FWHM of 113 meV at room temperature.

Figure 5-2..... 60

Current versus time behaviors during anodising of the Zn/Al bilayer in 0.3 M C₂H₂O₄ at constant 40V.

Figure 5-3..... 61

The top-view of SEM image after removed alumina films in process I in 0.3 M C₂H₂O₄ at constant 40V.

Figure 5-4..... 62

The AFM image of zinc oxide nanodot arrays.

Figure 5-5..... 63

TEM image of zinc oxide under alumina film. The inset is the SAED (selected area electron diffraction) image.

Figure 5-6..... 64

EELS spectrum of zinc oxide nanodot arrays under the porous alumina films.

